This is the author's version of a work that was submitted/accepted for publication in the following source:

This file was downloaded from: http://eprints.qut.edu.au/51333/

Prediction of Pull-out Force of Multiwall Carbon Nanotube (MWCNT) in Sword-in-sheath Mode

Go Yamamoto, Sen Liu, Ning Hu*, Toshiyuki Hashida, Yaolu Liu, Cheng Yan, Yuan Li, Hao Cui, Huiming Ning and Liangke Wu

G. Yamamoto, T. Hashida
Fracture and Reliability Research Institute, Tohoku University, 6-6-01 Aramaki-Aza-Aoba, Aoba-ku, Sendai 980-8579, Japan

S. Liu, N. Hu, Y. Liu, Hao Cui, Huiming Ning, Liangke Wu
Department of Mechanical Engineering, Chiba University, 1-33 Yayoi-cho, Inage-ku, Chiba 263-8522, Japan
E-mail: huning@faculty.chiba-u.jp

Cheng Yan
School of Engineering Systems, Queensland University of Technology, 2 George Street, G.P.O. Box 2434, Brisbane, Queensland 4001, Australia
E-mail: c2.yan@qut.edu.au

It is well-known that multi-wall carbon nanotubes (MWCNTs) are of a unique atomic structure which consists of multiple coaxial cylindrical walls with an approximate wall spacing of 0.34 *nm*. In general, the interaction between the walls is largely through weak van der Waals (vdW) force rather than chemical bonds. Therefore, some walls tend to slide easily against the others under external loading. It has been realized that the sliding between the walls can be used for some applications such as ultrahigh frequency longitudinal oscillators in a nano-electro-mechanical system (NEMS) [1-2]. In fact, the pull-out of outer walls against the inner walls has been frequently observed in MWCNTs under tensile [3-5]. This has also been confirmed from the fracture surfaces of various MWCNT-reinforced nanocomposites [6-9], referred as "*sword-in-sheath*" fracture. To date, due to the technical challenge for testing at nanoscale, limited experimental studies have been conducted on the wall sliding in MWCNTs [1-5]. In addition, numerical studies based on molecular mechanics (MM) or molecular dynamics (MD) have been carried out to understand the pull-out/sliding process [10-12]. Unfortunately, the pull-out forces numerically predicted [10-12] were generally much lower

than the experiment [1-5]. This was attributed to possible mechanical cross-links or interfacial frictional effect [11]. Anyway, quantitative analysis on pull-out is still lacking, despite the significance of associated technical problems such as suitability of MWCNTs as reinforcements in composites or as oscillators in microsystems. In this work, we conducted extensive experiment and MM simulations to gain a better understanding of the pull-out in MWCNTs. We found that the pull-out force is proportional to the diameter of the immediate outer wall on the sliding interface. More importantly, we also realized the capped section of the MWCNT plays a critical role in the pull-out process.

In previous work [10-12], the cap effect on the pull-out force has not been well explored, which we believe may contribute to the disagreement between the predicted pull-out force and the experimental measurements. To overcome this problem, we conducted MM simulations with emphasis on the effect of capped section of a MWCNT on the pull-out force. The basic idea of the present analysis is to evaluate the potential energy variation during a pull-out process. By neglecting some possible energy dissipations (e.g., thermal dissipation), the work done by the pull-out force and the variation of the potential energy can be used to work out the pull-out force. Firstly, a double-walled carbon nanotube (DWCNT) was modeled with a pull-out force F (**Figure 1**a). To simplify the analysis, the inner capped tube was divided into two parts, i.e., the completely embedded capped tube with a pull-out force F_1 (**Figure 1**b), and the partially embedded tube with a pull-out force F_2 (**Figure 1**c). The total pull-out force F is the sum of F_1 and F_2.

The analysis of the pull-out process (**Figure 1**b) was mainly divided into two steps: (1) the fixed boundary conditions were applied to the atoms of the outer cap (red atoms in **Figure 1**b), and then (2) the inner wall was pulled out step-by-step along the axial direction by applying a constant prescribed displacement increment Δx of 0.01 *nm* on the atoms of the left top end of the inner wall. After each pull-out step, the structure was relaxed to obtain the minimum potential energy E. In our previous work [12], it was found that pull-out force of an

2

uncapped DWCNT was only proportional to the diameter of the outer wall, and independent of the nanotube length and chirality. For this reason, the models with different diameters were built up to investigate the cap effect. The calculated energy increments (ΔE) between two consecutive pull-out steps of three DWCNTs is shown in **Figure 1**d where D is the diameter of the outer wall. Here, D is defined as the immediate outer wall at the sliding interface, i.e., "*diameter of sliding interface*". In **Figure 1**d, it can be seen that the energy increment ΔE increases rapidly up to a peak value at a specified displacement (labeled as Stage *I* in **Figure 1**d), and then keeps steady with increase of pull-out displacement (Stage *II* in **Figure 1**d). The peak value of ΔE also increases with D. The ΔE starts to decrease after reaching the peak value (Stage *III*). The same feature were also observed in the simulation of two other WCNTs with larger diameters, i.e., (54,54)/(59,59) with D of 8.0 *nm* and (83,83)/(88,88) with D of 11.933 *nm*. Corresponding to the Stage *II,* the maximum pull-out force can be evaluated by using the relationship between the potential energy variation and the work done by the pull-out force. The average maximum energy increment, i.e., ΔE_{max}, for the five DWCNTs with different D is shown in **Figure 1**e. The relationship between the ΔE_{max} and D can be perfectly fitted into a quadratic function (**Figure 1**e) as follows:

$$\Delta E_{max} = 2.09D^2 - 2.15D + 0.94 \qquad \text{(in kcal/mol with } \pm 10\% \text{ fitting error)} \qquad (1)$$

In fact, the maximum relative fitting error of Eq. (1) is 8.9% for the above five DWCNTs. For instance, the constant term of "0.94" in Eq. (1) should be a fitting error since ΔE_{max} should be zero for zero D.

To understand this potential energy increment in detail, we further divided the inner wall into two parts, i.e., the cap and the tube (**Figure 2**a). The corresponding pull-out forces for these two parts are F_1^1 and F_1^2, respectively and $F_1 = F_1^1 + F_1^2$. It was found that the energy increment shown in **Figure 1**d was dominated by the pull-out of the cap part. The pull-out of the inner tube did not affect the variation of the potential energy, i.e., $F_1^2 = 0$. The

reason can be explained using **Figure 2**b. If the length of the outer tube is long enough, the carbon atoms of the inner tube are always in force equilibrium. For example, in **Figure 2**b, the atoms in red are balanced by the symmetrical horizontal forces from the atoms of the outer wall, which are within the cut-off distance of Lennard–Jones potential. During a pull-out process, the relative motion of the atoms between the inner and outer walls creates repetitive breaking and reforming of the vdW interactions and no resultant resistance force can be generated on the inner tube. The quadratic form of the energy increment in Eq. (1) due to the cap effect is also associated with the surface energy density. Considering a cap model shown in **Figure 2**c, the bottom edge is just located on the boundary between the cap and the tube. If we use γ_{max} and γ_{min} to represent the maximum and minimum potential energy variation per unit area under a specified separation displacement, γ_{max} is at the top of the cap, and γ_{min} appears at the bottom. Then, the surface energy varies from the top to the bottom of the cap in a function of $\gamma(\phi) = \gamma_{max} \cos(90^{\circ} - \phi) = \gamma_{max} \sin \phi$, which implies that $\gamma_{min}=0$. This is reasonable as $F_1^2 =0$. The total surface energy of the cap can be calculated as

$$\varPsi_{cap} = \int_0^{2\pi} (\int_0^{\pi/2} \gamma(\phi) R \cos \phi \times R d\phi) d\theta = \frac{\pi D^2}{2} \int_0^{\pi/2} \gamma(\phi) \cos \phi d\phi = \frac{\pi D^2}{4} \gamma_{max} \qquad (2)$$

From Eq. (2), regardless of the function of $\gamma(\phi)$, the surface energy is always proportional to πD^2. As a result, the energy increment of the cap during the pull-out can be described by a quadratic function of D. Approximately, the γ_{max} at the small top area of the cap during pull-out process can be predicted in the same way as the separation of two flat graphite sheets (**Figure 2**d). This was confirmed by the similar displacement-energy increment curves obtained from the simulation of two graphite sheets. In Stage *II,* γ_{max} corresponding to the displacement increment of 0.01 *nm* was around 0.355 kcal/nm^2. Substituting this value into Eq. (2) leads to the total surface energy increment as $\varPsi_{cap} = 2.764 D^2$ (kcal/mol) under 0.01 *nm* displacement. This result is approximately

equivalent to Eq. (1) for ΔE_{max}, which again indicates that the quadratic form of Eq. (1) is appropriate. Note that the deformation mode significantly affects the value of γ_{max}. For instance, we also calculated the γ_{max} of the two graphite sheets in a pure shear separation mode. It was found that the γ_{max}^s under shear is about **3.54** times lower than the γ_{max} in the normal separation mode. This finding further highlights the contribution of the cap to ΔE_{max} not only from its large area ($\propto D^2$), but also from its higher energy density under normal separation mode.

After validating Eq. (1), it becomes easy to predict the pull-out force F_1. Corresponding to the stable Stage *II* in **Figure 1**d, the maximum pull-out force is simply evaluated by equaling the work done by the pull-out force and the ΔE_{max}, i.e.,

$$\Delta E_{max} = F_1 \times \Delta x, \tag{3}$$

where Δx is chosen as $0.01nm$, i.e., the pull-out displacement increment in Stage *II*, and then

$$F_1 = 1.451D^2 - 1.493D + 0.65 \tag{4}$$

where F_1 is of the unit of *nN*, and *D nm*.

For F_2 shown schematically in **Figure 1**c, our previous study showed, the potential energy change during the pull-out process was only dominated by the atoms located within an approximate range ± 1 *nm* centered by the left end of the outer wall [13]. From our previous work [12], this force was obtained to be proportional to *D* as follows

$$F_2 = 1.15D - 0.45 \tag{5}$$

Note that F_2 is much smaller than F_1, because of less atoms contributing to the vdW interactions and the much lower surface energy density under shear, as mentioned before. For the pull-out in **Figure 1**c, the systematic potential energy variation is, $\Psi_{exit} = (2\pi\gamma_2\Delta x)D = 1.27D$ (kcal/mol) corresponding to 0.01 *nm* displacement increment. Here γ_2 is obtained from our previous study [12]. Clearly, Ψ_{exit} is much lower than Ψ_{cap}.

Finally, the total pull-out force F (**Figure 1**a) was simply evaluated as

$$F = F_1 + F_2 = 1.451D^2 - 0.343D + 0.20 \qquad \text{(with } \pm 10\% \text{ fitting error))} \qquad (6)$$

Naturally, the above analysis is largely for DWCNTs. For MWCNTs, the sword-in-sheath fracture mode is categorized into the two simplified models, as shown in **Figure 2**e (Case 1) and **Figure 2**f (Case 2). Case 1 is a pull-out process at an arbitrary interface. As confirmed in Ref. 12 and 13, except for the immediate two outer and inner walls from the sliding interface, the contributions of other walls away from the sliding interface can be neglected. Therefore, we only considered the immediate two outer and two inner walls (**Figure 2**e). Case 2 denoted the sliding between the outmost wall and its adjacent inner wall. We only considered the immediate two inner walls and the outmost wall near the sliding interface. Using the existing results for F_2 [12], we conducted the simulation for F_1 in Cases 1 and 2 and the pull-out forces in the MWCNTs can be evaluated as

$$F_{MWCNT} = 1.29F \quad \text{(Case 1)} \quad \text{(with } \pm 10\% \text{ fitting error))} \qquad (7a)$$

$$F_{MWCNT} = 1.14F \quad \text{(Case 2)} \quad \text{(with } \pm 10\% \text{ fitting error)} \qquad (7b)$$

where F is the pull-out force for DWCNTs (Eq. 6). Note that the above empirical equations are only applicable for the sword-in-sheath fracture mode in a MWCNT. In some cases, the entire cross-section of MWCNTs can break under tension load [14].

To verify the simulation above, we performed the tensile test of MWCNTs. The MWCNT material (acquired from Nano Carbon Technologies Corporation; Tokyo, Japan) was synthesized by a catalytic chemical vapor deposition (CCVD) method followed by high temperature annealing. The typical diameter and length of the pristine MWCNTs measured by scanning electron microscopy (SEM, Hitachi S-4300) and transmission electron microscopy (TEM, Hitachi HF-2000) are in the range of 33~124 *nm* (70 *nm* in average) and 1.1 to 22.5 *μm* (average: 8.7 *μm*) (**Figure 3**a), respectively. Some pristine MWCNTs were refluxed in a concentrated H_2SO_4: HNO_3 (3:1 volume ratio) mixture at 70°C for 2 h, washed thoroughly

with distill water, and then finally dried in air at 60°C. Some "channel-like" defects around the circumference of the MWCNTs were observed after the acid-treatment, as shown in **Figure 3**b. Tensile tests of individual MWCNTs were performed with a nanomanipulator [4, 15] inside the vacuum chamber of a SEM (FEI Quanta 600 FEG). The details of the tensile experiment are described elsewhere [5]. Ten pristine MWCNTs and ten acid-treated MWCNTs were tested and they all failed in the sword-in-sheath mode. As shown in **Figures 3**c, d, e and f, for a typical sample after acid-treatment, the sword and sheath parts can be clearly identified. The diameter of the sword part (Ds) of each MWCNT was measured using SEM at a magnification of 100,000, **Figure 3**f.

The pull-out forces measured experimentally are compared with the prediction using Eqs. 7(a) and 7(b), as shown in **Figure 3**g. It can be seen that the pull-out force for the acid-treated MWCNTs is lower than that of pristine ones with the same diameter. Firstly, the original diameters of MWCNTs D_0 was used for the prediction. Although the numerical prediction for Cases 1 and 2 pass catches the trend of the experimental evaluation, a data scattering is observed as shown in the inset of **Figure 3**g. Instead, we used the "*diameter of sliding interface*", i.e., D, which is equal to $Ds+0.68$ *nm* as the wall space is about 0.34 *nm* and a better agreement between the experimental and numerical prediction is achieved for both the pristine and acid-treated MWCNTs. The experimental observation indicates that most samples fall into the Case 1 failure pattern but the Case 2 pattern is still possible, confirmed by the observation in a few samples. For the acid-treated MWCNTs, the sword-in-sheath fracture generally starts from the "channel-like" defects (**Figure 3**b). On the other hand, for the pristine MWCNTs, we need to double check whether or not the analysis can be applied to the particular case where the outmost walls break before the sword-in-sheath type pull-out can be triggered. Based on our previous experiment [5], the tensile load needed to break 10 outmost walls of the MWCNTs (average diameter 70 *nm*) is only around 1300 *nN*, which is much lower than the pull-out force obtained in the present work (**Figure 3**g). This confirms

the current analysis is valid for both the pristine and acid treated MWCNTs. In addition, we also compared the numerical results with other experimental results [1-3] and a good agreement has been observed (**Figure 3**g), which further validates the effectiveness of the proposed empirical formulas.

In conclusion, based on experiment and detailed MM simulations, the present work proposed an empirical theory for prediction of the pull-out forces in DWCNTs and MWCNTs, provided they fail in a sword-in sheath mode. We found that the pull-out force is dominated by the contribution from the capped section of a carbon nanotube due to larger number of atoms and higher surface energy density. This finding fully explained the controversial results recently observed in evaluation of pull-out phenomenon in carbon nanotubes and provides a basis for further investigation on the complicated interactions between carbon nanotube and other materials such as polymers.

_[1]   S. Akita, Y. Nakayama, *Jpn. J. Appl. Phys.* **2003**, *32*, 3933.

_[2]   J. Cumings, A. Zettl, *Science* **2000**, *289*, 602.

_[3]   M.F. Yu, B.I. Yakobson, R.S. Ruoff, *J. Phys. Chem. B* **2000**, *104*, 8764.

_[4]   M.F. Yu, O. Lourie, M.J. Dyer, K. Moloni, T.F. Kelly, R.S. Ruoff, *Science* **2000**, *287*, 637.

_[5]   G. Yamamoto, J.W. Suk, J. An, R.D. Piner, T. Hashida, T. Takagi, R.S. Ruoff, *Diam. Relat. Mater.* **2010**, *19*, 748.

_[6]   G. Yamamoto, K. Shirasu, T. Hashida, T. Takagi, J.W. Suk, J. An, R.D. Piner, R.S. Ruoff, *Carbon* **2011**, *49*, 3709.

_[7]   H.D. Wagner, O. Lourie, Y. Feldman, R. Tenne, *Appl. Phys. Lett.* **1998**, *72*, 188.

_[8]   B. Peng, M. Locascio, P. Zapol, S. Li, S.L. Mielke, G.C. Schatz, H.D. Espinosa, *Nat.*

Nanotech. **2008**, *3*, 626.

_[9] W. Ding, A. Eitan, F.T. Fisher, X. Chen, D. Dikin, R. Andrews, L.C. Brinson, L.S. Schadler, R.S. Ruoff, *Nano Lett.* **2003**, *3*, 1593.

_[10] Q. Zheng, J.Z. Liu, Q. Jiang, *Phys. Rev. B* **2002**, *65*, 245409-1.

_[11]   Z. Xia, W.A. Curtin, *Phys. Rev. B* **2004**, *65*, 233408-1.

_[12] Y. Li, N. Hu, G. Yamamoto, Z. Wang, T. Hashida, H. Asanuma, C. Dong, M. Arai, H. Fukunaga, *Carbon* 2010, *48*, 2934.

_[13]   S. Liu, N. Hu, G. Yamamoto, Y. Cai, Y. Zhang, Y. Liu, Y. Li, T. Hashida, H. Fukunaga, *Carbon* **2011**, *49*, 3698.

_[14] A.H. Barber, R. Andrews, L.S. Schadler, H.D. Wagner, *Appl. Phys. Lett.* **2005**, *87*, 203106.

_[15] W.Q. Ding, L. Calabri, X.Q. Chen, K.M. Kohhaas, R.S. Ruoff, *Compos. Sci. Technol.* **2006**, *66*, 1112.

_[16] W. Ding, D.A. Dikin, X. Chen, R.D. Piner, R.S. Ruoff, E. Zussman, X. Wang, X. Li, *J. Appl. Phys.* **2005**, *98*, 014905.

_[17] J.E. Sader, J.W.M. Chon, P. Mulvaney, *Rev. Sci. Instrum.* **1999**, *70*, 3967.

_[18] F. Deng, *Thesis of PhD.*, Tokyo University, **2008**.

_[19] Y. Li, Y. Liu, X. Peng, C. Yan, S. Liu, N. Hu, *Comput. Mater. Sci.* **2011**, *50*, 1854.

_[20] S.J.V. Frankland, A. Caglar, D.W. Brenner, M. Griebel, *J. Phys. Chem. B* **2002**, *106*, 3046.

Figure 1. MM simulation of pull-out process. a) Schematic diagram of a DWCNT model; b) sub-problem 1 of a); c) sub-problem 2 of a); d) MM results of b) for energy increment versus pull-out displacement; e) relationship between CNT diameter and maximum energy increment in Stage II.
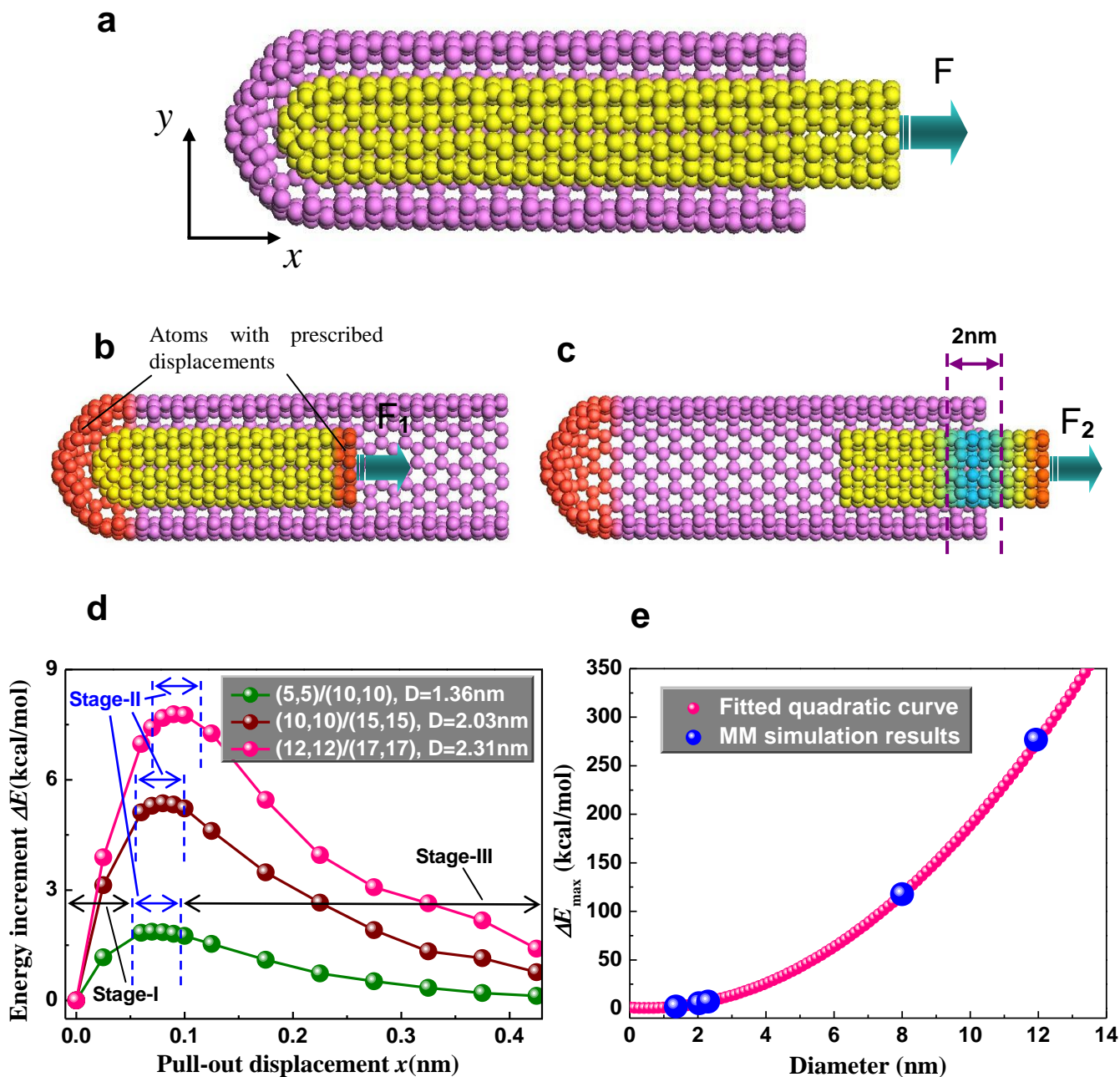
Figure 2. Schematic diagram for discussion on MM results and models of MWCNTs. a) decomposition of sub-problem 1 in Figure 1b); b) force state of a tube part only; c) estimation of energy variation of a cap area; d) two graphite sheets for calculating γ_{max}; e) schematic diagram for the first simplified case of MWCNT (Case 1); f) schematic diagram for the second simplified case of MWCNT (Case 2).
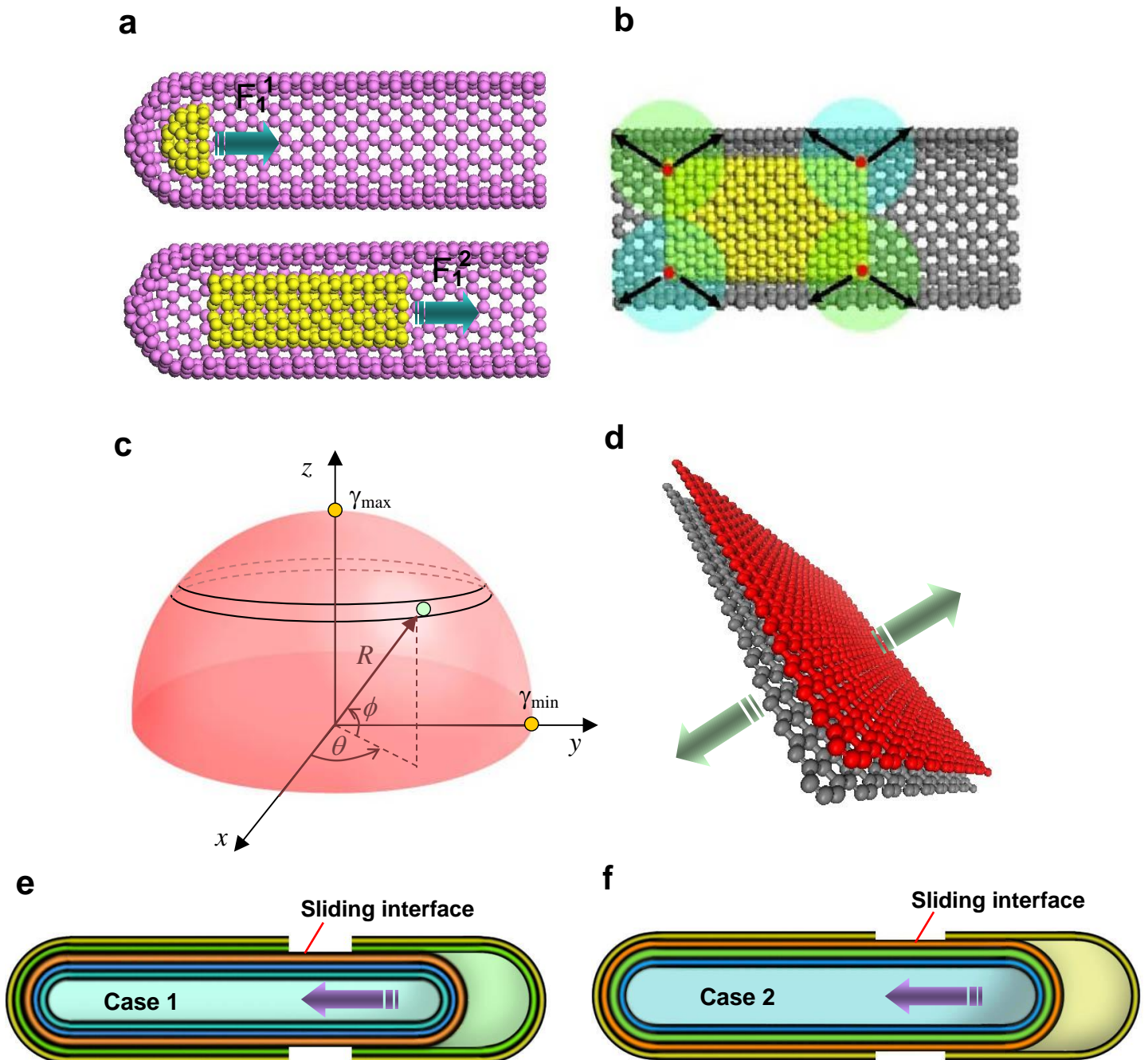
Figure 3. Experiments and verification of numerical results. a) TEM picture of a pristine MWCNT; b) TEM picture of an acid-treated MWCNT; c) SEM picture of tensile experiment; d) sword part of the MWCNT in c) after test; e) sheath part of the MWCNT in c) after test; f) enlarged illustration of d); g) comparison between numerical and experimental results